Science Advances
AAAS

advances.sciencemag.org/cgi/content/full/6/26/eaba9624/DC1

Supplementary Materials for

A breathable, biodegradable, antibacterial, and self-powered electronic skin based on all-nanofiber triboelectric nanogenerators

Xiao Peng, Kai Dong, Cuiying Ye, Yang Jiang, Siyuan Zhai, Renwei Cheng, Di Liu,
Xiaoping Gao, Jie Wang*, Zhong Lin Wang*

*Corresponding author. Email: wangjie@binn.cas.cn (J.W.); zhong.wang@mse.gatech.edu (Z.L.W.)

Published 26 June 2020, *Sci. Adv.* **6**, eaba9624 (2020)
DOI: 10.1126/sciadv.aba9624

This PDF file includes:

Figs. S1 to S33
Notes S1 to S7

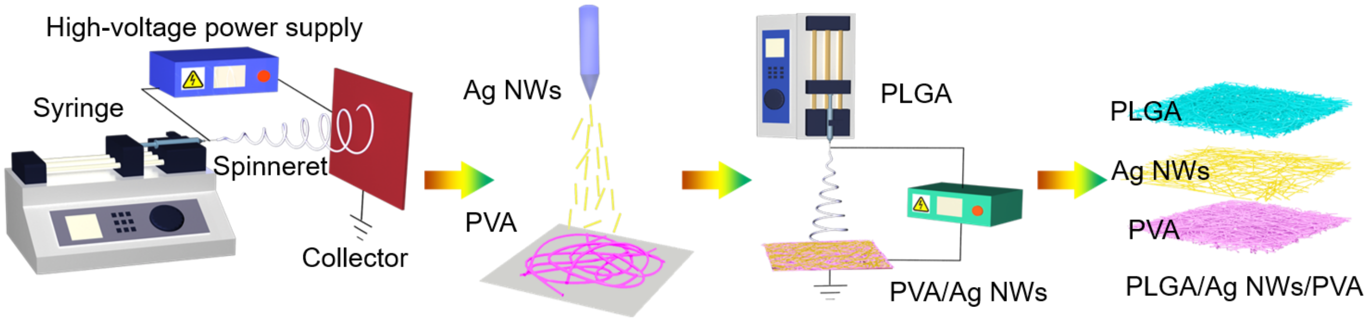

Fig. S1. Fabrication process of the PLGA/Ag NWs/PVA nanofiber TENG-based electronic skin.

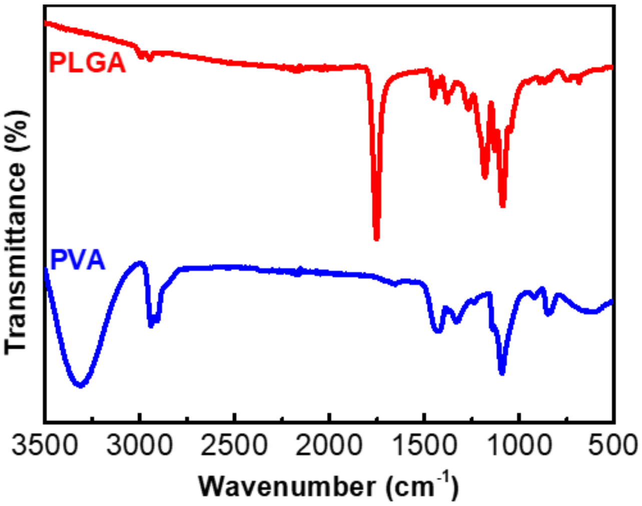

Fig. S2. Fourier transform infrared (FTIR) spectra of PLGA and PVA nanofiber films.

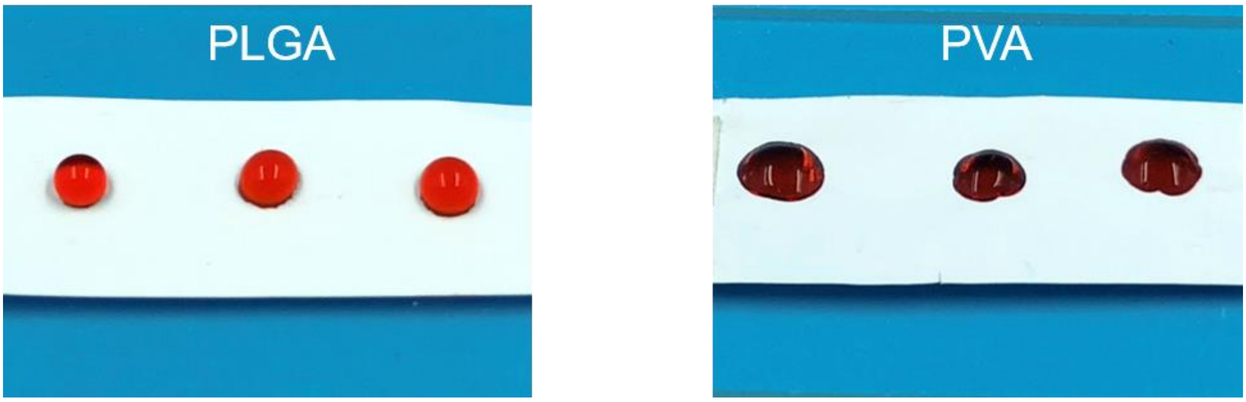

Fig. S3. Hydrophobic property of PLGA nanofiber film (contact angle = 115°) and hydrophilic property of PVA nanofiber film (contact angle = 38°). Photo Credit: Xiao Peng, Beijing Institute of Nanoenergy and Nanosystems.

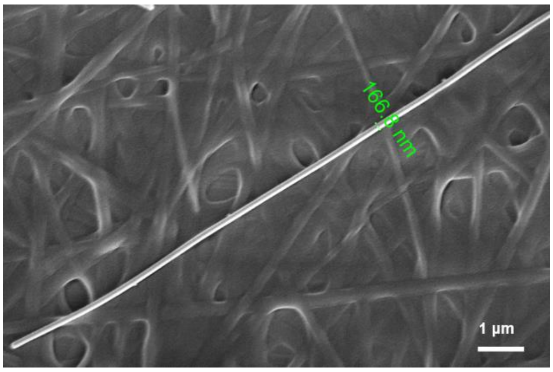

Fig. S4. SEM image of a single Ag nanowire (NW) with the diameter of about 167 nm.

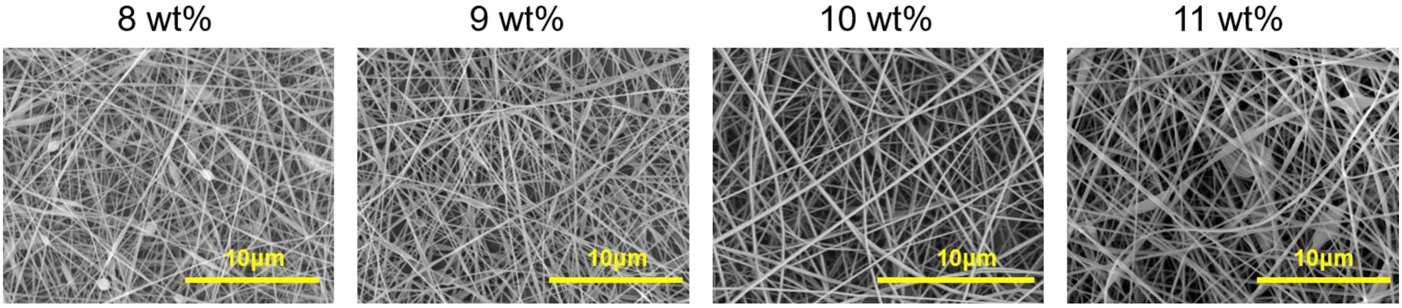

Fig. S5. SEM images of the PVA electrospun nanofibers under different PVA solution concentrations. It is found that the uniformity of PVA nanofibers is poor and string beads appear when the concentration is low. However, if the concentration is a little higher, the solution viscosity increases and the difficulty of electrospinning will also increase, which leads to the poor uniformity of PVA nanofiber film. Therefore, 10 wt% is the optimal solution concentration for the PVA electrospun nanofiber film.

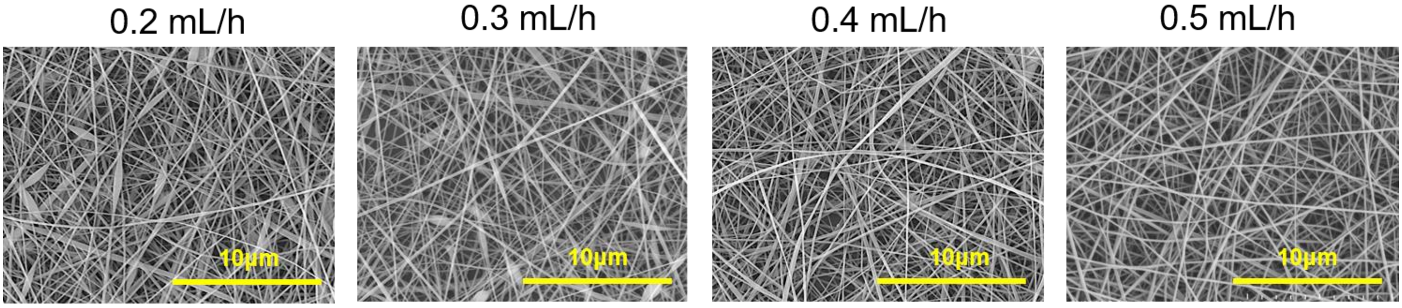

Fig. S6. SEM images of the PVA electrospun nanofibers under different solution flow rates.

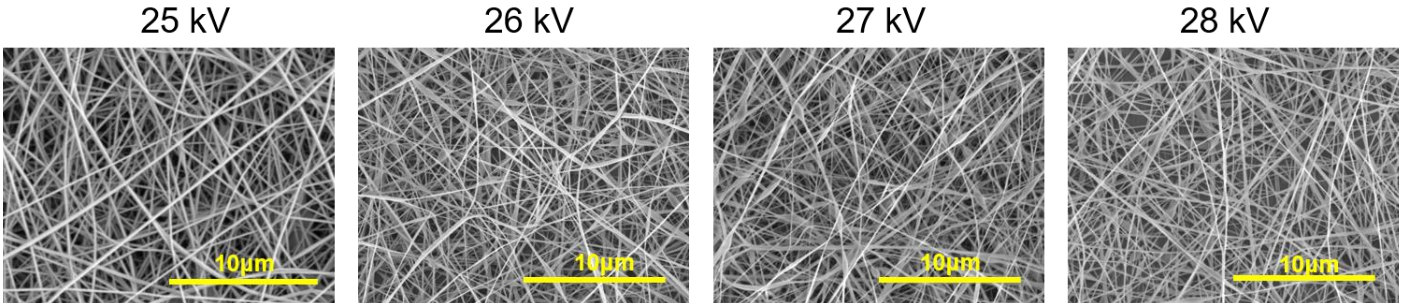

Fig. S7. SEM images of the PVA electrospun nanofibers under different applied voltages.

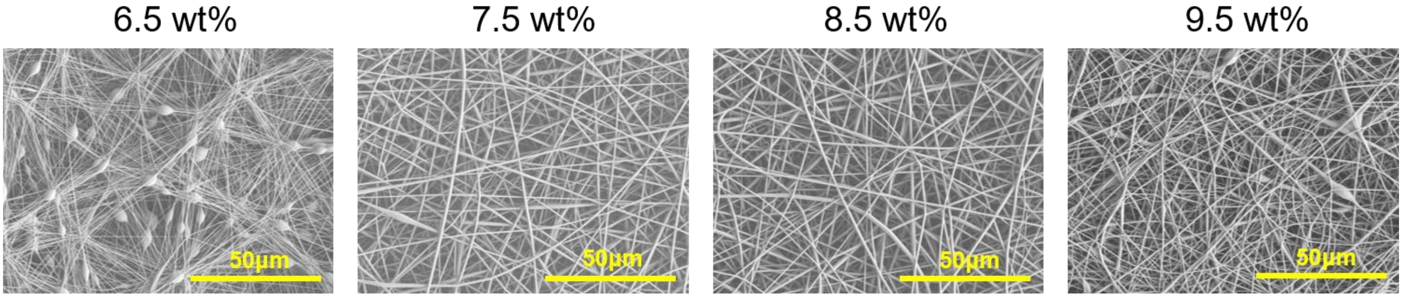

Fig. S8. SEM images of the PLGA electrospun nanofibers under different PLGA solution concentrations.

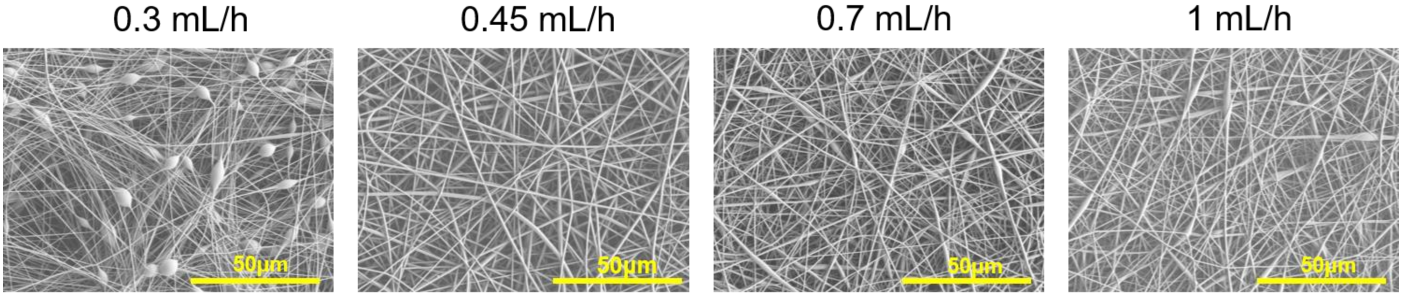

Fig. S9. SEM images of the PLGA electrospun nanofibers under different solution flow rates.

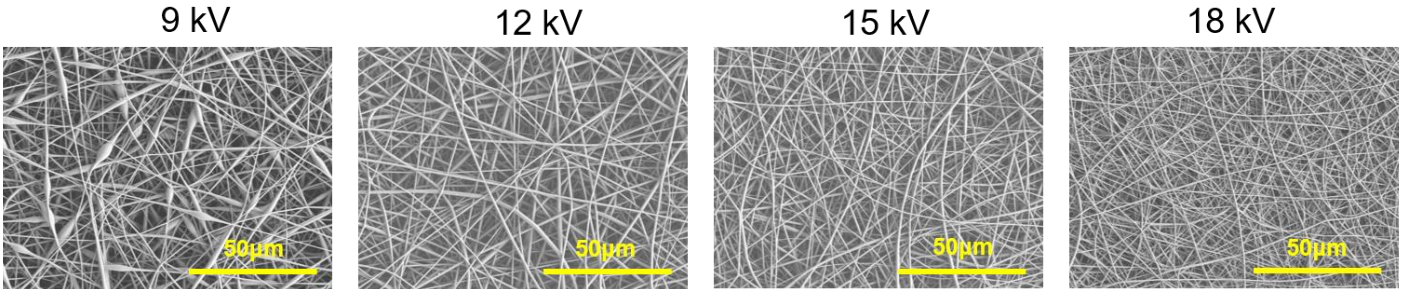

Fig. S10. SEM images of the PLGA electrospun nanofibers under different applied voltages.

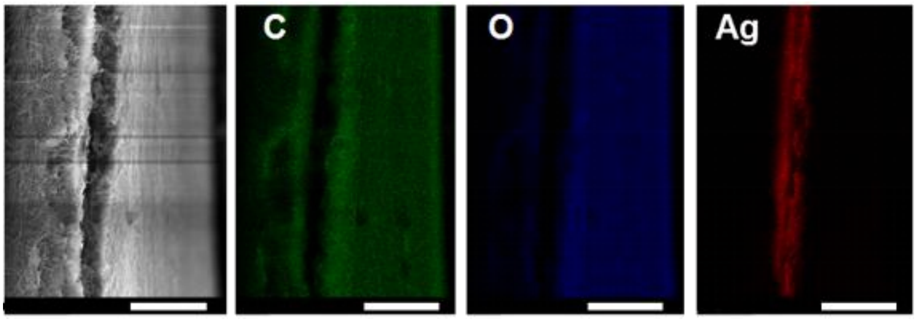

Fig. S11. Cross-sectional SEM image with EDX elemental mappings of the all nanofiber TENG-based e-skin after 90 days of exposure in air atmosphere and four hours of breath operation (scale bar: 50 µm).

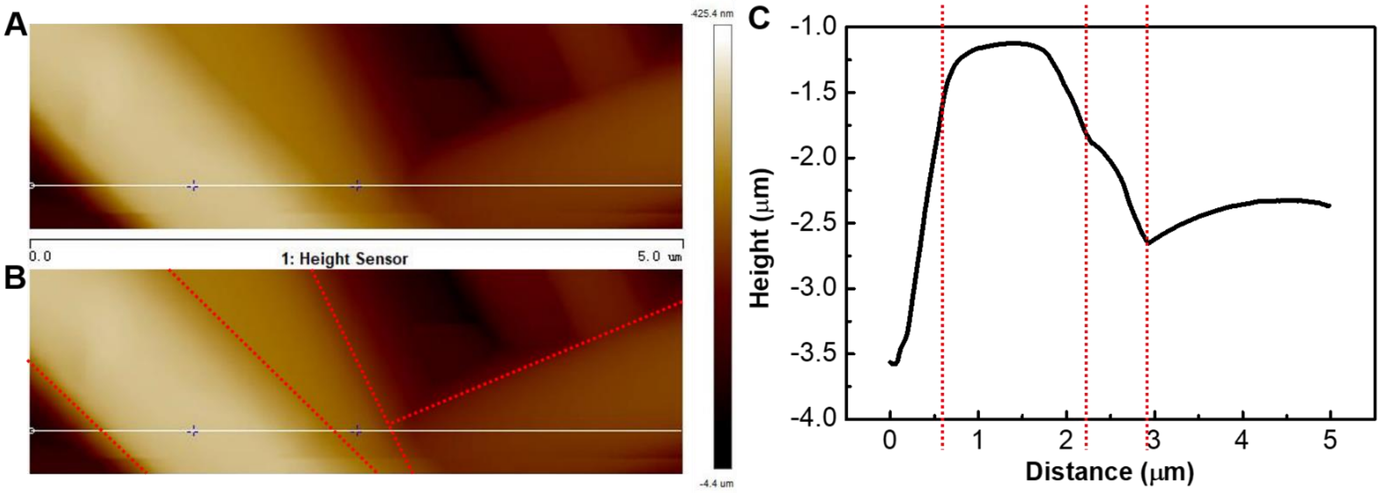

Fig. S12. Atomic force microscopy (AFM) analysis of the surface of PLGA nanofiber film. (A) AFM image **(B)** Regional division in the AFM image. **(C)** Height distribution along the white line in (a) and (b).

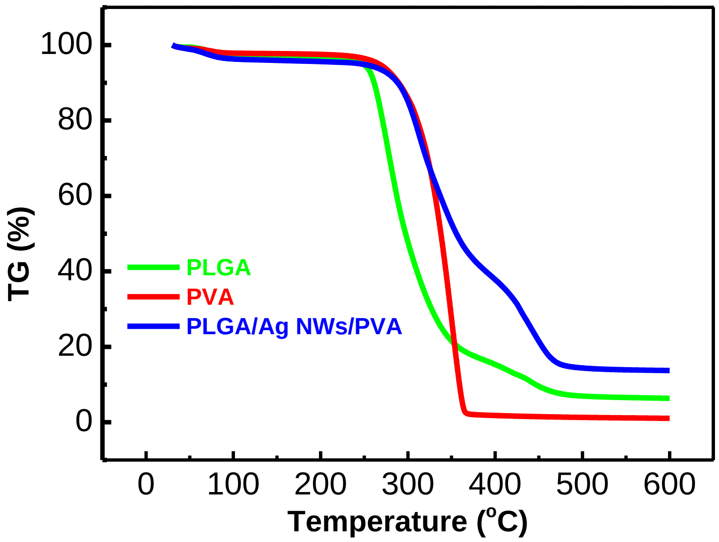

Fig. S13. Thermogravimetric (TG) analyses of the PLGA, PVA and PLGA/Ag NWs/ PVA nanofiber films.

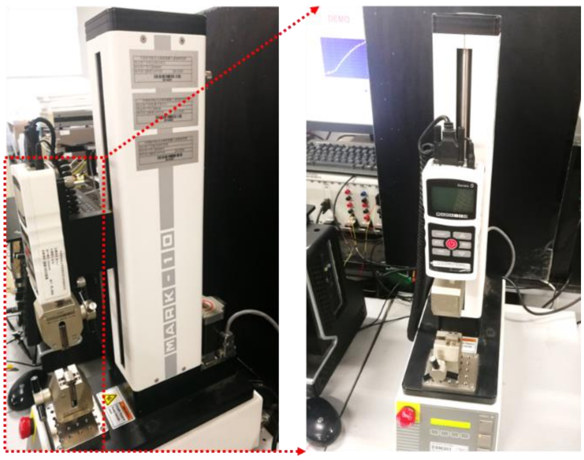

Fig. S14. Photographs of the uniaxial tensile tester for nanofiber films. Photo Credit: Xiao Peng, Beijing Institute of Nanoenergy and Nanosystems.

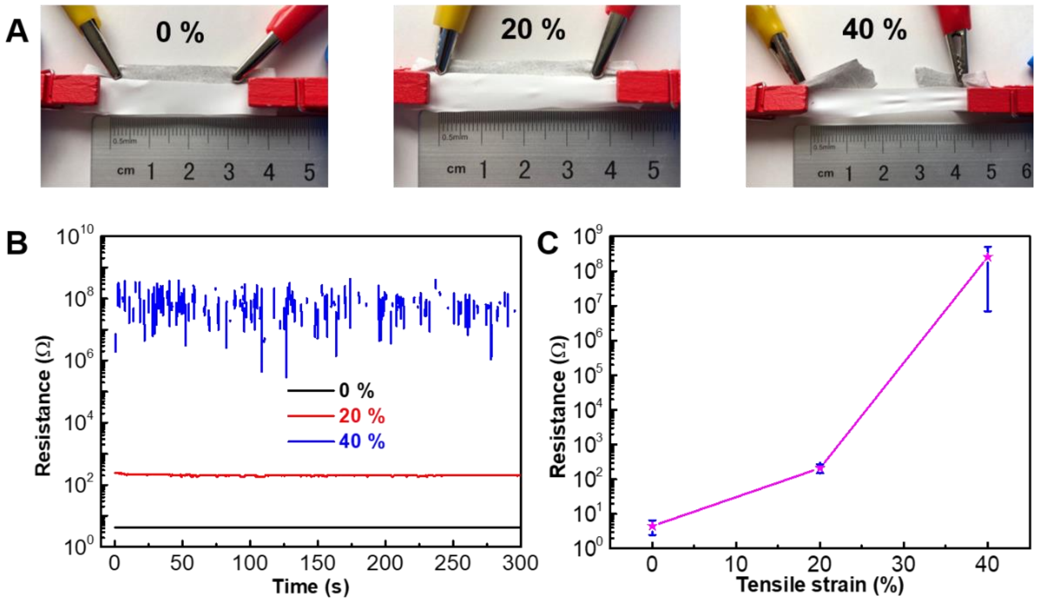

Fig. S15. Effect of tensile strain levels on the electric resistance of the PLGA/Ag NWs/PVA nanofiber film. (**A**) Photograph images of PLGA/Ag NWs/PVA nanofiber film under different tensile strain levels. (**B**) Stability analyses of PLGA/Ag NWs/PVA nanofiber film under different tensile strain levels. (**C**) Relationship between tensile strains and electric resistances. Photo Credit: Xiao Peng, Beijing Institute of Nanoenergy and Nanosystems.

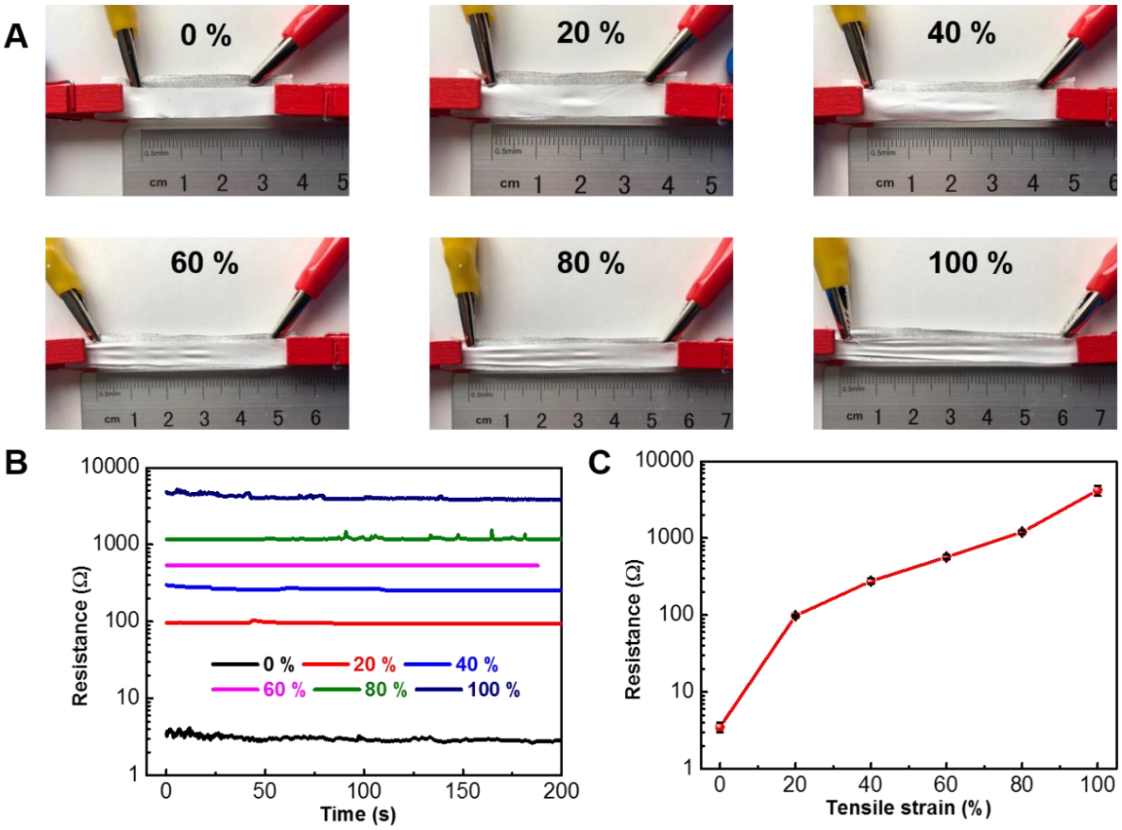

Fig. S16. Effect of tensile strain levels on the electric resistance of the PLGA/Ag NWs/PLGA nanofiber film. (**A**) Photograph images of PLGA/Ag NWs/PLGA nanofiber film under different tensile strain levels. (**B**) Stability analyses of PLGA/Ag NWs/PLGA nanofiber film under different tensile strain levels. (**C**) Relationship between tensile strains and electric resistances. Photo Credit: Xiao Peng, Beijing Institute of

Nanoenergy and Nanosystems.

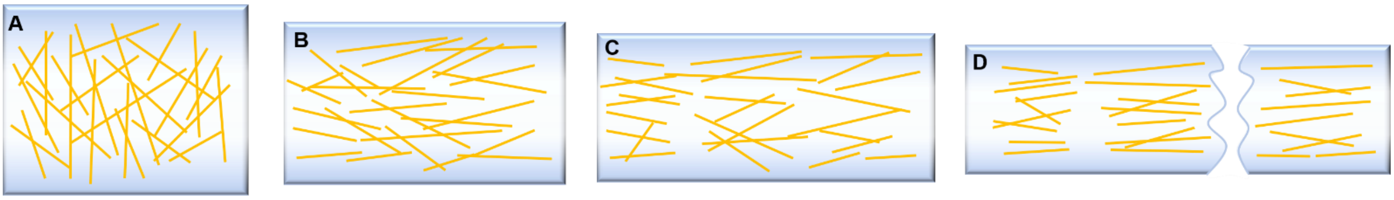

Fig. S17. The potential reasons and mechanisms of the electric resistance variations of Ag NWs deposited films under different tensile strains.

Fig. S18. Photographs of the air permeability tester for nanofiber films. Photo Credit: Xiao Peng, Beijing Institute of Nanoenergy and Nanosystems.

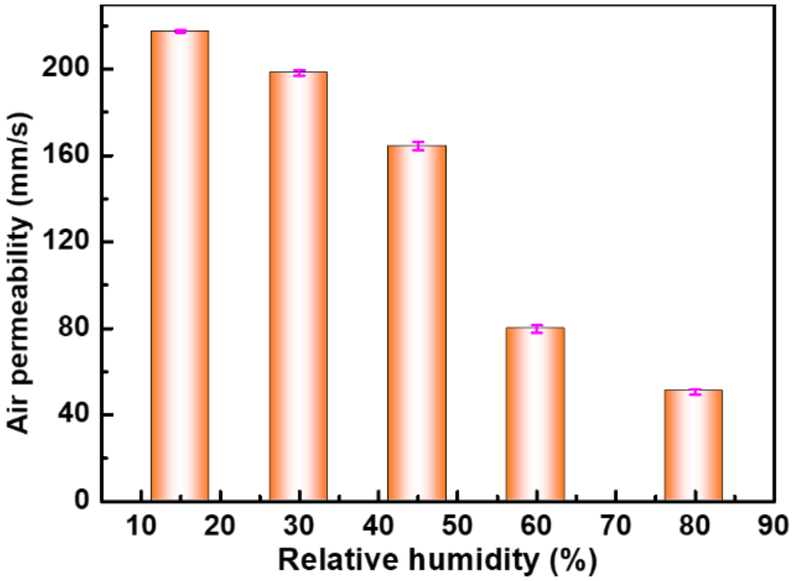

Fig. S19. Air permeability of the PLGA/Ag NWs/PVA e-skin under different environmental humidity (15%, 30%, 45%, 60% and 80%). The total thickness of the test TENG is about 40 μm, and the applied force is 200 Pa. All the sample were pre-conditioned in a constant temperature and humidity chamber for 24 hours. The setting temperature is 25 °C, and the humidity is set as 15%, 30%, 45%, 60% and 80%, respectively.

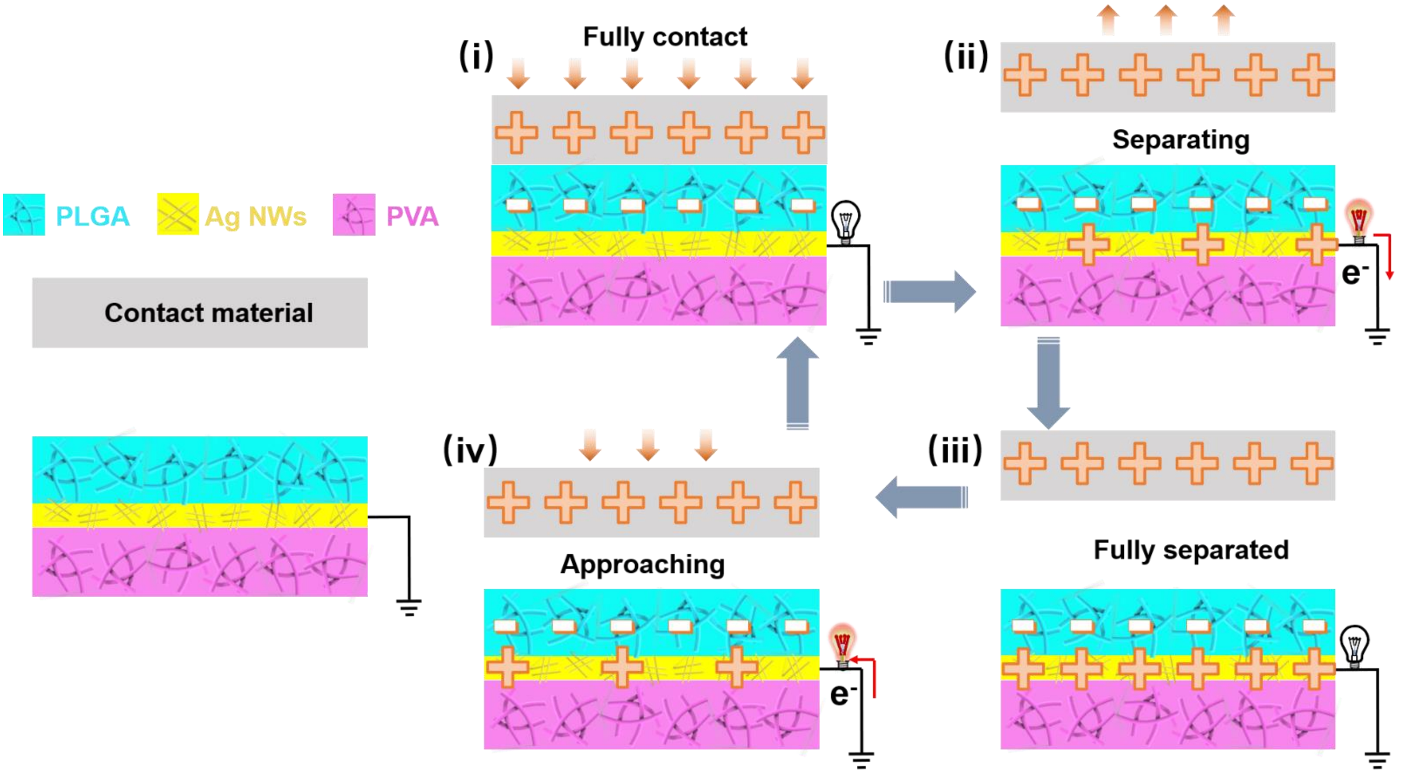

Fig. S20. Schematic illustration of the working mechanism of the all-nanofiber TENG-based e-skin in a complete contact-separation cycle, including (i) fully contact, (ii) gradually separating away, (iii) fully separated, and (iv) gradually approaching to.

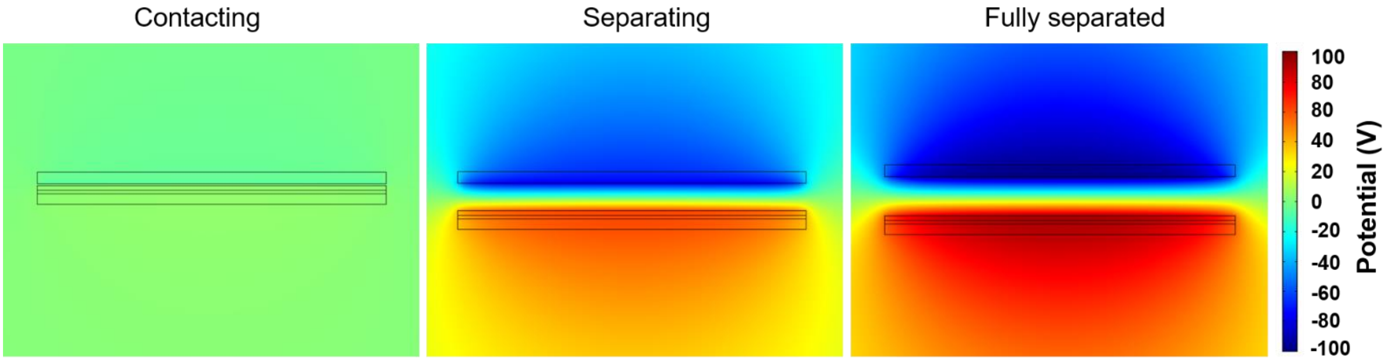

Fig. S21. Potential simulation by COMSOL to elucidate the working principle of the all-nanofiber TENG-based e-skin.

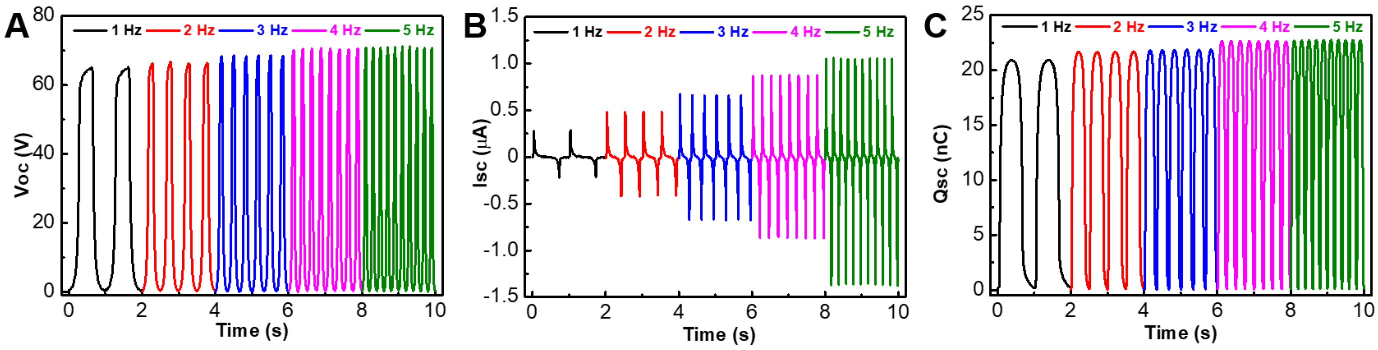

Fig. S22. Electrical output performance of the PVA/Ag NWs/PVA e-skin under different loading frequencies (1-5 Hz), including (A) VOC, (B) ISC and (C) QSC.

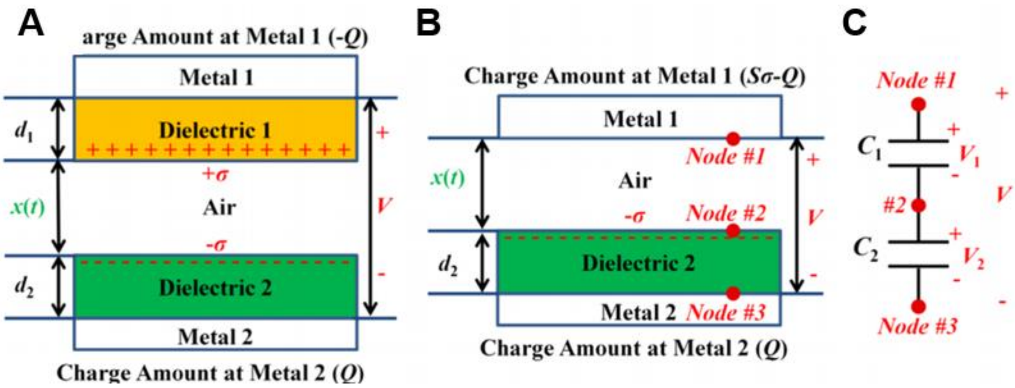

Fig. S23. Theoretical models for (**A**) dielectric-to-dielectric attached-electrode parallel-plate contact-mode TENG and (**B**) Conductor-to-dielectric attach-electrode parallel-plate contact-mode TENGs. (**C**) Equivalent circuit diagram for conductor-to-dielectric attach-electrode parallel-plate contact-mode TENG *(1)*.

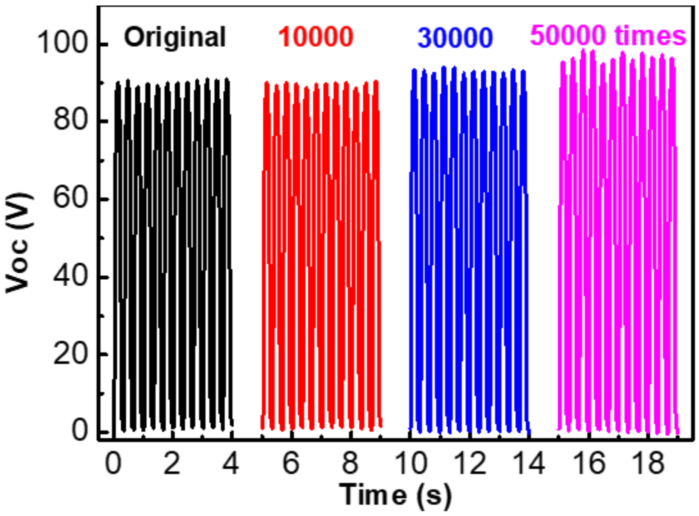

Fig. S24. Long-term durability of the all-nanofiber TENG-based e-skin for more than 50,000 cycles of contact-separation motions.

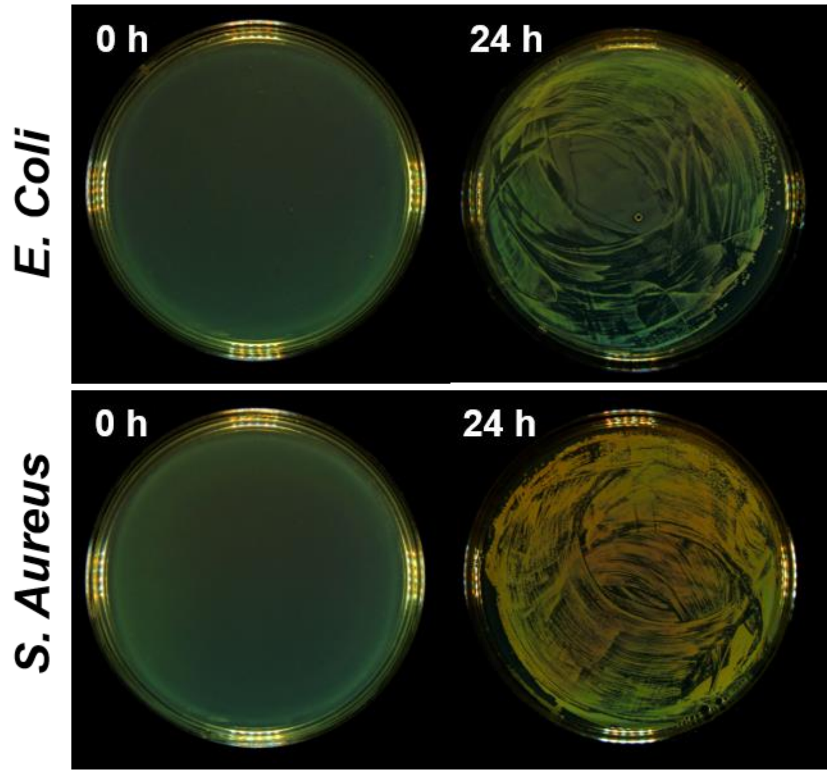

Fig. S25. Colonies of bacteria of *E. coil* and *S. aureus* on blank agar plates before and after incubation for 24 h.

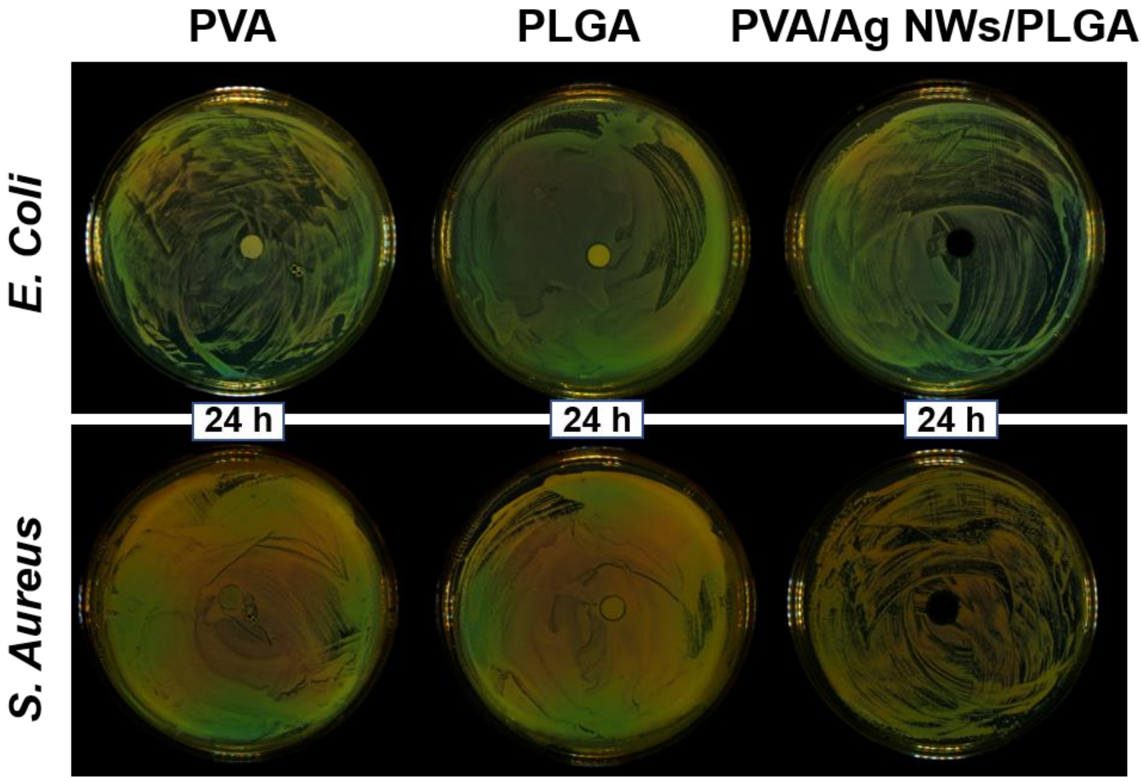

Fig. S26. Inhibition zones of the PVA, PLGA, and PLGA/Ag NWs/PVA nanofiber films against *E. coil* and *S. aureus* after incubation for 24 h.

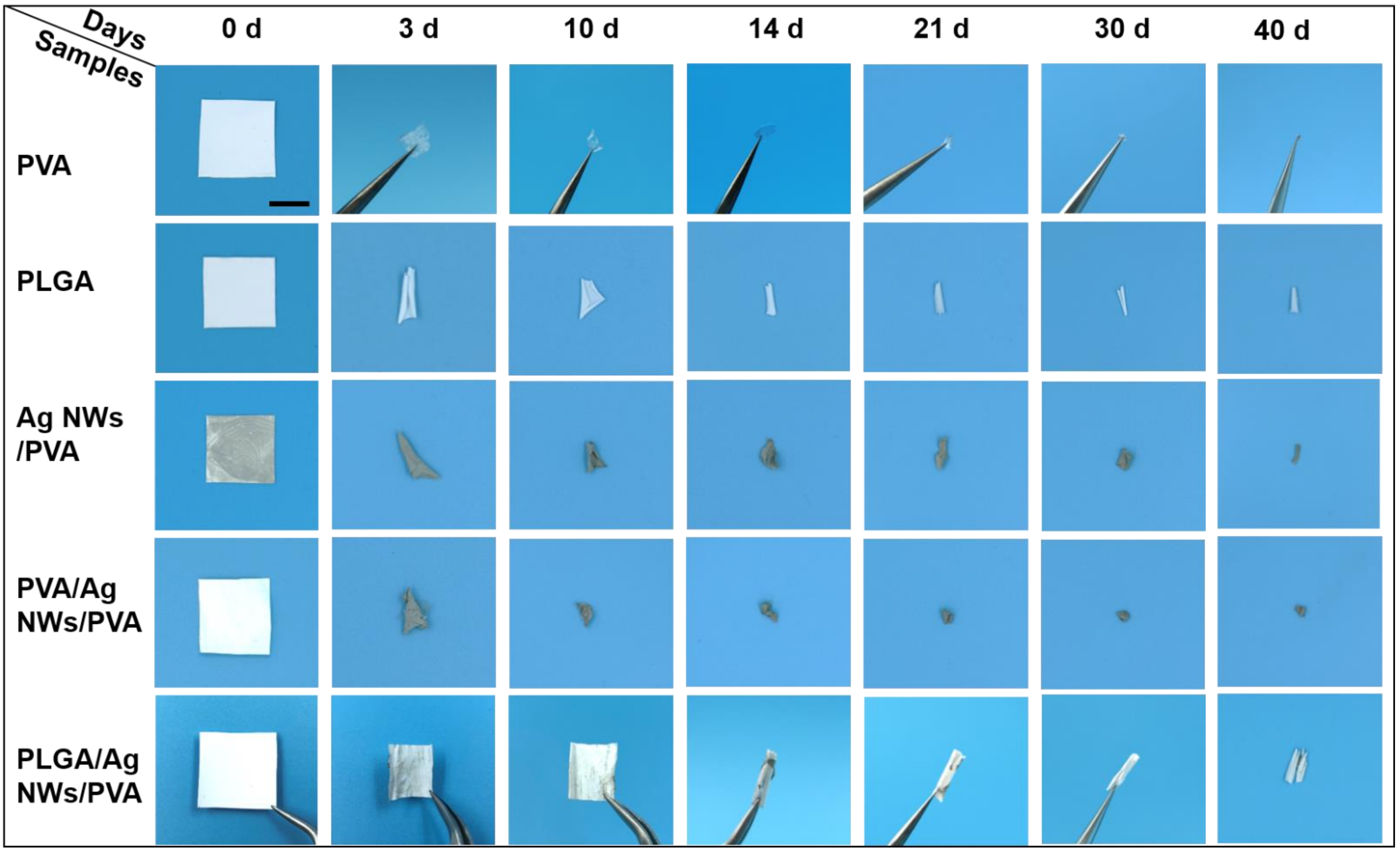

Fig. S27. In-vitro biodegradation processes in PBS solution of PVA, PLGA, Ag NWs/PVA, PVA/Ag NWs/PVA, PLGA/Ag NWs/PVA nanofiber films within the degradation cycles of 40 days (scale bar: 1 cm). Photo Credit: Xiao Peng, Beijing Institute of Nanoenergy and Nanosystems.

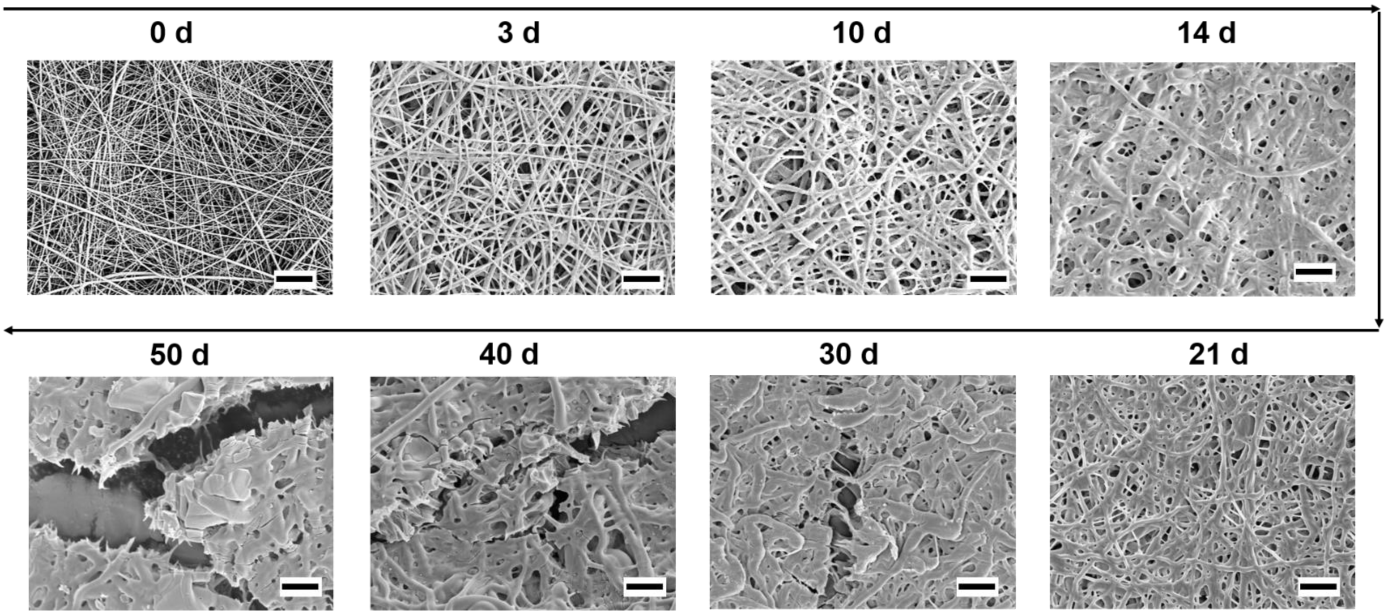

Fig. S28. SEM images of PLGA nanofiber films under different degradation periods (scale bar: 5 μm).

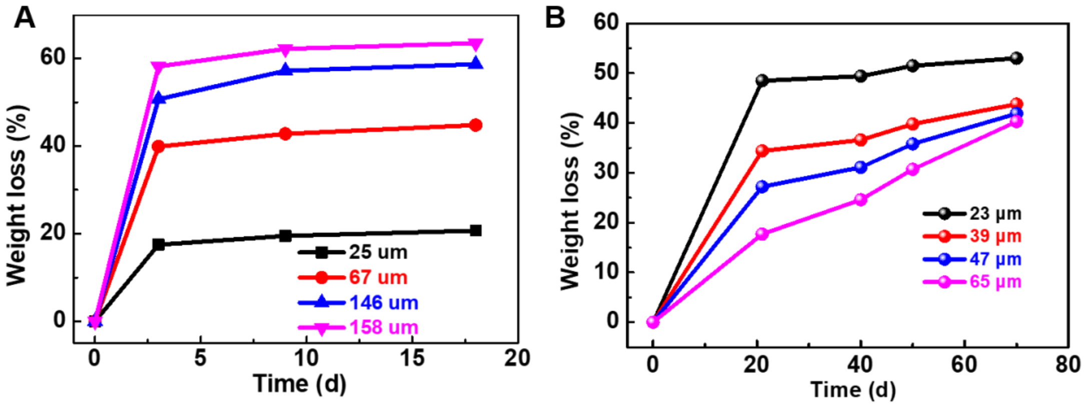

Fig. S29. Effect of the thickness of (A) PVA film and (B) PLGA film on the degradation time of the PLGA/Ag NWs/PVA e-skin. It is worth noting that the marked values are only the thickness of (**A**) PVA film and (**B**) PLGA film, but the weight loss rates belong to the whole PLGA/Ag NWs/PVA device.

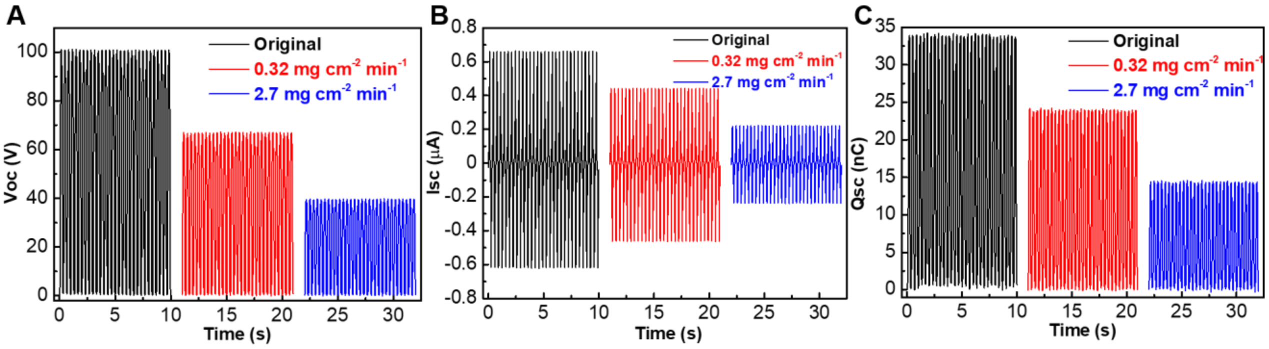

Fig. S30. Effect of sweat on electrical output performance of all nanofiber TENG-based e-skin.

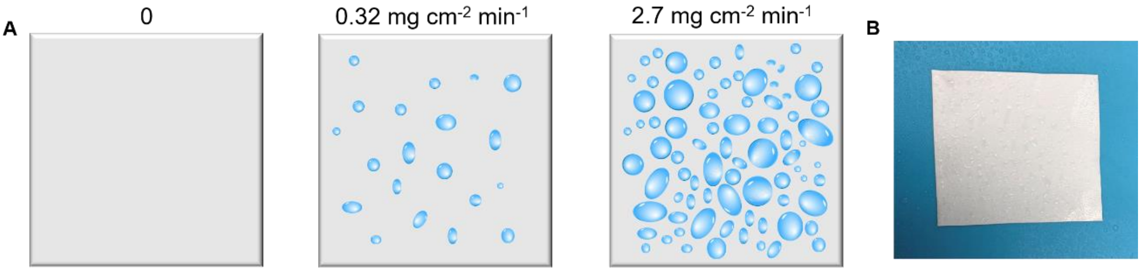

Fig. S31. (A) Schematic illustration of sweat on the PLGA/Ag NWs/PVA e-skin. (B) Photograph of sweat on PVA nanofiber film with the maximum amount of sweat rate (about 2.7 mg cm^{-2} min^{-1}). The artificial sweat was prepared according to ISO 3160-2 standard, including 20 g/L sodium chloride (NaCl), 17.5 g/L ammonium chloride (NH4Cl), 5 g/L urea, 2.5 g/L acetic acid (CH3COOH), 15 g/L lactic acid, 80 g/L sodium hydroxide (NaOH) for adjusting the pH value to 4.7, and DI water. According to previous study *(45)*, it can be found that the minimum amount of sweat for the human body is about 0.32 mg cm^{-2} min^{-1}, and the maximum amount of sweat is about 2.7 mg cm^{-2} min^{-1}. Photo Credit: Xiao Peng, Beijing Institute of Nanoenergy and Nanosystems.

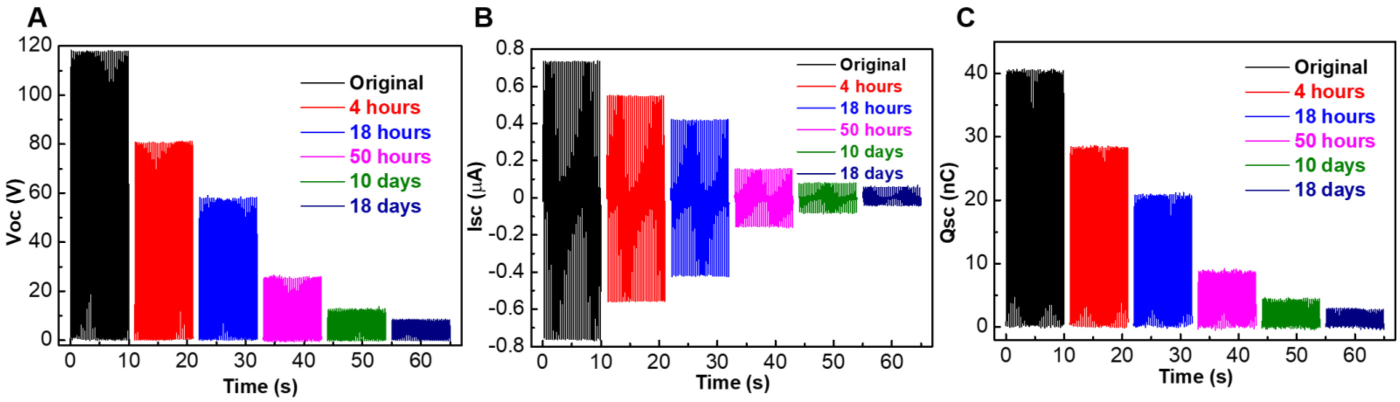

Fig. S32. Electrical output performance including (A) V_{OC}, (B) I_{SC}, and (C) Q_{SC} of the PLGA/Ag NWs/PVA e-skin under different degradation time. The applied force and frequency are 40 N and 3 Hz, respectively. It can be found that the electrical outputs of TENG decrease gradually with the increase of degradation time. In the degradation process, the delamination between PVA film and PLGA film will appear first, which will weaken their binding ability and affect the effective charge transfer. In addition, PVA film begins to shrink gradually, resulting in the decrease of effective contact area. In practical application, the TENG device will not be directly immersed in PBS solution, so its actual performance degradation time will be very long.

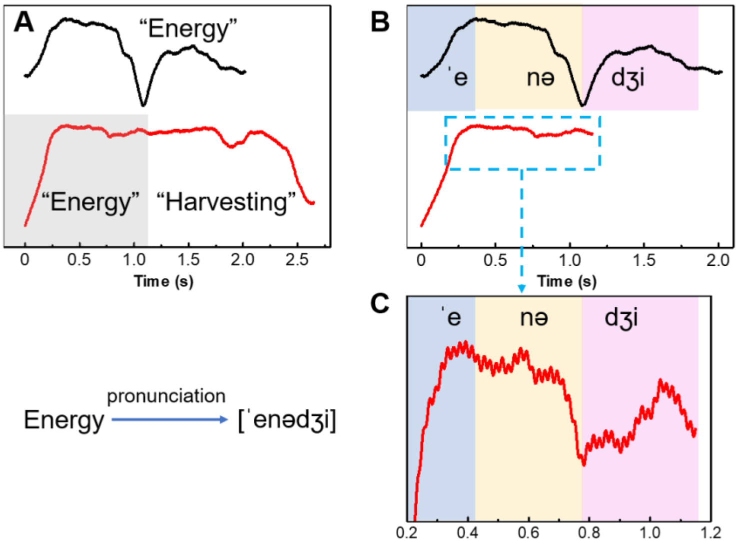

Fig. S33. Comparison of electrical output signals of speaking “Energy” and its extended phrase of “Energy harvesting”. The regions marked with blue, yellow and pink represent the voltage signals generated by the pronunciation of “ˈe”, “nə” and “dʒi”, respectively.

Note S1. Oxidation resistance analysis of Ag NWs after prolonged exposure to air and even a period of respiratory operation

The SEM images in **fig. S11** are the EDX analysis on the PLGA/Ag NWs/PVA e-skin after 90 days of exposure in air atmosphere and four hours of breathing operation. The specific operation process is as follows: we first selected the remaining PLGA/Ag NWs/PVA nanofiber film for EDX analysis, which has been placed in the air environment for more than 90 days. Then, the nanofiber film was placed at the vent of a mask for 4 hours circulatory breathing operation. From these SEM images, it is difficult to find oxygen (O) element at the middle Ag NWs electrode, which further verifies the stability (no oxidation) after long-term exposure to air and circulatory breathing operation.

Note S2. Variations of electrode resistance of our e-skins under different tensile strain levels

As shown in **Figure 2A**, the PLGA/Ag NWs/PVA nanofiber film has two fracture processes. Considering the tensile strength of PVA is weaker than that of PLGA, PVA film will break first, and then PLGA film breaks. The maximum tensile strain of the composite nanofiber film is about 30 %. **fig. S15** shows the variation of electric resistance of the PLGA/Ag NWs/PVA nanofiber film with tensile strains from 0 % to 40 %. The initial resistance of the Ag NWs deposited PVA film is as low as several ohms. In addition, resistance increases significantly with the increase of tensile strain. When the tensile strain reaches 40 %, Ag NWs deposited PVA film breaks and resistance increases to hundreds of megaohms.

As shown in **Figure 2A**, the PLGA/Ag NWs/PLGA nanofiber film also has two fracture processes. Due to the deposition of Ag NWs, PLGA nanofiber film will slightly shrink and compact, which has higher tensile strength than pure PLGA nanofiber film. Therefore, the Ag NWs deposited PLGA nanofiber film will break first, and then pure PLGA nanofiber film. **fig. S16** shows the electric resistance changes of the PLGA/Ag NWs/PLGA nanofiber film under the tensile strain from 0 % to 100 %. Due to the tensile fracture strains of both the Ag NWs deposited PLGA nanofiber film and pure PLGA nanofiber film are more than 100 %, the fracture strain of the composite PLGA/Ag NWs/PLGA nanofiber film will also exceed 100 % (**Figure 2A**). It can be found that the resistances of the PLGA/Ag NWs/PLGA nanofiber film increase with the increase of tensile strain. Moreover, all the resistances have good stability in a period of time (200 s).

The increase of resistance with the tensile strains can be explained by the following model (**fig. S17**). Initially, Ag NWs deposited in polymer films are randomly arranged and effectively connected, which forms a good conductive network (**fig. S17A**). Therefore, the resistance is rather low. When the film is stretched, its width decreases and its length increases. Moreover, Ag NWs are gradually oriented along the stretching direction (**fig. S17B**). Under this circumstance, most of Ag NWs are still in connected state, which will not greatly increase resistance. As the tensile continues, the conductive network is blocked due to the disconnection of most Ag NWs (**fig. S17C**). In this case, the resistance will increase significantly. Once the film is broken, the conductive channel will disappear completely (**fig. S17D**). Therefore, the resistance will be quite large and even close to insulation state.

Note S3. Thermal-moisture stability and comfortability of the all-nanofiber TENG-based e-skin

The schematic illustration in the top left of **Fig. 2C** is a simplified view of the cross section of the PLGA/Ag NWs/PVA e-skin, in which the red, yellow and green solid circles refer to the PVA, Ag NWs and PLGA, respectively. The red and black dotted arrows represent the gas or water molecules flowing from the environment to the skin and from the skin to the environment, respectively.

The heat or moisture transfer occurs once there is a temperature or humidity gradient between the human skin and the external environment. The system between the human skin and the external environment is also called as human microenvironment. On one hand, PLGA nanofiber film is hydrophobic that can effectively prevent large water molecules from penetrating into the electrode. However, micro/nanopores are widely distributed in its surface, enabling air and small molecules to pass. On the other hand, PVA nanofiber film is environmentally friendly and hydrophilic that can quickly absorb the heat and sweat from the body and discharge them out timely. When the surface temperature or humidity in the human body is higher than that in the outside, such as in motion, the gas and moisture molecules will flow from skin surface through interfiber capillary channels to the environment, as the path of the black dotted lines.

Note S4. Electricity generation principle of the all-nanofiber TENG-based e-skin

The all-nanofiber TENG-based e-skin will work in a single-electrode mode when the middle Ag NWs electrode is connected to the ground through external resistances (**fig. S20**). One cycle of contact electrification process corresponds to a complete contact-separation movement occurring between the e-skin and external contact materials (e.g. skin, latex, or acrylic). Taking the human skin as the external contact material for example, surface charge transfer occurs at their interface when they come into contact with each other due to the combined effect of contact electrification and electrostatic balance, which results in the human skin losing electron on its surface, and PLGA triboelectric layer gaining electrons from its surface (**fig. S20i**). As they are only confined to the interface, charges with opposite signs coincide at the same plane, leading to no electric potential difference between the two surfaces. When they are separating and gradually moving away, a potential difference is established considering the Ag NWs electrode has no net charge while the PLGA layer has negative charges. Due to the electrostatic induction effect, the potential difference prompts positive charges to flow from the ground to the inner Ag NWs electrode, which generates an instantaneous current (**fig. S20ii**). When the two layers are completely separated, the negative charges in the PLGA layer are fully equilibrated by the electrostatic induced charges on the Ag NWs electrode (**fig. S20iii**). In this case, electrical signal is absent, reflecting the neutralization of charges. It should be noted that the accumulated charges will not be entirely annihilated. Instead, they will be maintained for a sufficiently long time due to the innate features of insulator. In the reverse case, if they are approaching back, the accumulated positive charges in the Ag NWs electrode flow back to the ground through the external load to compensate for electrical potential differences (**fig. S20iv**). After the whole system returns to the initial state, the negative charges on the PLGA layer are fully offset by the positive charges on the external skin again (**fig. S20i**). As a result, a contact-separation process between the human skin and the TENG-based e-skin will generate an instantaneous alternating potential and current through the external load.

Note S5. The relationship between loading frequency and electrical output performance (V_{OC}, Q_{SC} and I_{SC})

The models built for dielectric-to-dielectric and conductor-to-dielectric contact-mode TENGs are shown in **fig. S23A** and **S23B**, respectively. The V-Q-x relationship for the contact-mode TENGs can be derived based on electrodynamics. Therefore, the basic equation is given by *(39)*:

$$V = -\frac{Q}{S\varepsilon_0}\left(d_0 + x(t)\right) + \frac{\sigma x(t)}{\varepsilon_0} \tag{S1}$$

The output voltage (V_{OC}) for an open circuit, the transferred charge (Q_{SC}), and the output current (I_{SC}) in short-circuit conditions are as follows *(39)*:

At open-circuit condition, there is no charge transfer, which means

$$V_{OC} = \frac{\sigma x(t)}{\varepsilon_0} \tag{S2}$$

At short-circuit condition, V is 0. Therefore, the transferred charges are

$$Q_{SC} = \frac{S\sigma x(t)}{d_0 + x(t)} \tag{S3}$$

$$I_{SC} = \frac{dQ_{SC}}{dt} = \frac{S\sigma d_0}{\left(d_0 + x(t)\right)^2}\frac{dx}{dt} = \frac{S\sigma d_0 v(t)}{\left(d_0 + x(t)\right)^2} \tag{S4}$$

where S is the triboelectric surface area. x(t) is the time-dependent distance between the two triboelectric layers. ε_0 is the permittivity of free space, σ is the tribo-charge surface density, and v(t) is the speed of the relative mechanical movement. The effective dielectric thickness d_0 is defined as the summation of all the thickness of the dielectric d_i between the two metal electrodes divided by its relative effective thickness ε_{ri} (**fig. S23C**), as shown below:

$$d_0 = \sum_{i=1}^{n} \frac{d_i}{\varepsilon_{ri}} \tag{S5}$$

From **equations S2** and **S3**, it can be found that the V_{OC} and Q_{SC} are independent of speed, which means that the variation of movement frequency will cause no change of the V_{OC} and Q_{SC}. However, the I_{SC} depends on the relative movement speed, which presents a positive correlation feature with the increase of speed.

Note S6. Analysis of higher electron transfer quantity of PLGA than that of PVA (PTFE is adopted as counter friction layer)

Previous study *(40)* has shown that when Kapton was used as the counter friction layer, PLGA has higher ability to obtain positive charge or lose electrons than PVA. Transferred charges of PLGA as the surface friction layer are also more than those of PVA as the surface friction layer. Based on the quantified triboelectric series *(41)* as well as **Figure 2L** in this manuscript, Kapton and PTFE have similar triboelectrification properties when contacting with PVA and PLGA.

In addition, by comparing **Figure 2D-F** with **fig. S22**, it can be found that PTFE contacting with PLGA/Ag NWs/PVA film shows higher electrical output than PTFE contacting with PVA/Ag NWs/PVA film. Therefore, when PTFE is taken as the counter friction layer, PLGA has better charge transfer ability than PVA (under the same film size and measurement conditions).

Note S7. Degradation time of our e-skin under different film thickness

Here, we mainly consider the influence of the thickness of PVA film and PLGA film. First of all, we chose the same size (2 × 2 cm^2) but different thickness of PVA film to prepare the PLGA/Ag NWs/PVA e-skin. The thicknesses of PLGA film and Ag NWs layer are kept the same as much as possible. The result shows that the degradation trend of different PVA film thickness is basically the same. Moreover, the thicker PVA film is, the greater the weight loss of TENG is (**fig. S29A**).

We also chose the same size (2 × 2 cm^2) but different thickness of PLGA film to analyze the effect of PLGA. The thicknesses of PVA film and Ag NWs layer are kept the same as much as possible. As shown in **fig. S29B**, in the early 21 days, the weight loss of the TENG is attributed to the degradation of PVA/Ag NWs. When the thickness of the PVA/Ag NWs film is fixed, the thicker the PLGA film is, the smaller the proportion of the PVA/Ag NWs in the whole device is. However, when the degradation time exceeds 21 days, PLGA films begin to degrade. The thicker the PLGA film is, the greater change rate of weight loss is.

Obviously, the degradation cycle or time of our all nanofiber TENGs is changeable, which can be achieved by adjusting the proportion of PVA and PLGA in the whole device. In addition, it should be noted that the above degradation tests are also conducted in PBS solution.